REPORT DOCUMENTATION PAGE

Form Approved
OBM No. 0704-0188

Report Date.	3. Report Type and Dates Covered.
1994	Final - Journal Article

4. Title and Subtitle.
Magnetospheric and Ionospheric Signals in Magnetic Observatory Monthly Means: Electrical Conductivity of the Deep Mantle

5. Funding Numbers.

Program Element No.	0601153N
Project No.	03204
Task No.	360
Accession No.	DN258032
Work Unit No.	574506503

6. Author(s).
McLeod, Malcolm G.

7. Performing Organization Name(s) and Address(es).
Naval Research Laboratory
Mapping, Charting and Geodesy Branch
Stennis Space Center, MS 39529-5004

8. Performing Organization Report Number.
Journal of Geophysical Research, Vol. 99, No. B7, pp. 13,577-13,590, July 10, 1994

9. Sponsoring/Monitoring Agency Name(s) and Address(es).
Naval Research Laboratory
Center for Environmental Acoustics
Stennis Space Center, MS 39529-5004

10. Sponsoring/Monitoring Agency Report Number.
NRL/JA/7442--93-0012

11. Supplementary Notes.

12a. Distribution/Availability Statement.
Approved for public release; distribution is unlimited.

12b. Distribution Code.

13. Abstract *(Maximum 200 words).*

First differences of magnetic observatory monthly means for 1963-1982 were analyzed using techniques of spherical harmonic analysis and power spectral analysis. The external source signal is shown to be primarily zonal in geomagnetic coordinates. Prominent peaks are present in the power spectrum at frequencies of 1.0 cycle/yr and 2.0 cycles/yr. The annual signal is largest on the degree 2 external zonal spherical harmonic, while the semiannual signal is largest on the degree 1 and degree 3 external zonal spherical harmonics. The presence of the semiannual signal on odd-degree spherical harmonics and of the annual signal on even-degree spherical harmonics was predicted from symmetry considerations and of the annual cycle of solar inclination. These signals are all modulated by the sunspot frequency and its harmonics. The degree 1 term is believed to be due mainly to magnetopause and ring currents while the degree 2 and degree 3 terms are believed to be due mainly to ionospheric currents. The degree 1 external zonal harmonic has a continuous spectrum in addition to the semiannual spectral peak. A corresponding degree 1 internal term is due to electromagnetic induction. The degree 1 continuous spectrum is useful for study of the electrical conductivity of the deep mantle. A global geomagnetic response function consistent with a mantle conductivity of about 10 S/m at the core-mantle boundary has been derived.

14. Subject Terms.
Geomagnetism; Magnetic Observatory Monthly Means; Harmonic Analysis; Spectral Analysis

15. Number of Pages.
14

16. Price Code.

17. Security Classification of Report.	18. Security Classification of This Page.	19. Security Classification of Abstract.	20. Limitation of Abstract.
Unclassified	Unclassified	Unclassified	SAR

JOURNAL OF GEOPHYSICAL RESEARCH, VOL. 99, NO. B7, PAGES 13,577–13,590, JULY 10, 1994

Magnetospheric and ionospheric signals in magnetic observatory monthly means: Electrical conductivity of the deep mantle

Malcolm G. McLeod
Naval Research Laboratory, Stennis Space Center, Mississippi

Abstract. First differences of magnetic observatory monthly means for 1963–1982 were analyzed using techniques of spherical harmonic analysis and power spectral analysis. The external source signal is shown to be primarily zonal in geomagnetic coordinates. Prominent peaks are present in the power spectrum at frequencies of 1.0 cycle/yr and 2.0 cycles/yr. The annual signal is largest on the degree 2 external zonal spherical harmonic, while the semiannual signal is largest on the degree 1 and degree 3 external zonal spherical harmonics. The presence of the semiannual signal on odd-degree spherical harmonics and of the annual signal on even-degree spherical harmonics was predicted from symmetry considerations and the annual cycle of solar inclination. These signals are all modulated by the sunspot frequency and its harmonics. The degree 1 term is believed to be due mainly to magnetopause and ring currents while the degree 2 and degree 3 terms are believed to be due mainly to ionospheric currents. The degree 1 external zonal harmonic has a continuous spectrum in addition to the semiannual spectral peak. A corresponding degree 1 internal term is due to electromagnetic induction. The degree 1 continuous spectrum is useful for study of the electrical conductivity of the deep mantle. A global geomagnetic response function consistent with a mantle conductivity of about 10 S/m at the core-mantle boundary has been derived.

Introduction

The geomagnetic field at Earth's surface consists of two parts: a part due to sources within Earth's surface and a part due to sources outside Earth's surface. These two parts of the geomagnetic field can in principle be separated from each other by the method of spherical harmonic analysis developed in 1838 for the magnetic potential function by C. F. Gauss. This method is based on the assumption that no significant electric currents cross Earth's surface.

External sources of the geomagnetic field include electric current systems within Earth's magnetosphere and ionosphere and on the magnetospheric boundary, which is called the magnetopause [*Potemra*, 1991; *Russell and Luhmann*, 1991]. All of the external current systems vary with time because of varying solar activity. Study of that portion of the geomagnetic field due to external sources can reasonably be expected to yield information on such geophysical parameters as ionospheric ionization and its time variations. This information can in turn be expected to contribute to understanding of the mechanisms by which ionization is created in the ionosphere.

Time variations of the external electric current systems produce time-varying magnetic fields that induce electric currents within Earth by electromagnetic induction. *Schuster* [1889] demonstrated the possibility of obtaining knowledge of the radial distribution of Earth's electrical conductivity from observations of time variations of the geomagnetic field due to external sources. The geomagnetic response function for a given degree spherical harmonic is defined as the transfer function between the induced internal spherical harmonic and inducing external spherical harmonic; the existence of a conductivity which is a function only of radial distance and which relates the current density linearly to the electric field is assumed.

Much of the methodology associated with estimation of geomagnetic response functions is due to *Banks* [1969]. Banks showed that for periods greater than a day and less than a year the geomagnetic spectrum is primarily due to a degree 1 external field aligned with Earth's magnetic dipole axis. He showed that in addition to a continuous spectrum there are discrete annual and semiannual lines in the spectrum and that the annual line is primarily a degree 2 external spherical harmonic aligned with Earth's magnetic dipole axis. This confirmed results of an extensive analysis by *Currie* [1966]. Currie concluded that ionospheric dynamo action is probably responsible for the annual variation, while a ring current located about 3.5 Earth radii from Earth's center is the most likely source of the semiannual line. The semiannual line had been previously resolved by *Eckhardt et al.* [1963]. Banks thought, as did Currie, that the ring current was the source of the external degree 1 spectrum. However, the next section will show that there are reasons to believe that at least part of the external degree 1 spectrum is due to electric currents on the magnetopause.

Achache et al. [1981] discussed the numerical computation of the geomagnetic response function from Earth's conductivity profile. They computed the degree 1 response function for three conductivity profiles previously proposed by *McDonald* [1957], *Banks* [1969], and *Ducruix et al.* [1980]. They compared computed values of the response function with values determined from measurements by other investigators for periods ranging from 20 days to 9

Paper number 94JB00728.

years. They concluded that the profile proposed by *Ducruix et al.* [1980] best fit the experimental data, but they stressed the need for more accurate determination of Earth's response at low frequencies, particularly periods of a few years. *McLeod* [1992] determined the response function for a 2-year period using magnetic observatory annual means for 1962–1983 as a data source. He concluded that the profile proposed by *Banks* [1969] fit this new result better than the other two profiles considered by *Achache et al.* [1981]. The Banks profile is for a conductivity of approximately 10 S/m at the core-mantle boundary.

Constable [1993] proposed a global geomagnetic response function, sensitive to average radial electrical conductivity of Earth's mantle between 200 and 2000 km, obtained by averaging response functions published by *Roberts* [1984] and *Schultz and Larsen* [1987]. The averages used in Constable's study were estimates for periods ranging from 3.25 days to 3.4 months. His response function is consistent with a conductivity jump at a depth of 660 km from a value of 2 S/m below 660 km to a much smaller value above this boundary. The boundary at 660 km corresponds to a seismic discontinuity and a presumed phase transition for mantle material. *Constable* [1993] gives several references for recent work on mineral physics and geomagnetic induction in the upper mantle.

Another approach to the determination of mantle conductivity involves measurement of the spectrum of signals that originate in Earth's core. If the spectrum of the signals at the base of the mantle is known (or assumed), then the radial electrical conductivity profile can be estimated from measurements of the spectra of these signals at Earth's surface. The basic problem with this approach is that the spectrum of the input at the base of the mantle is not known. A variation of this approach that uses assumed properties of the geomagnetic jerk of 1969 has been discussed by *Backus* [1983].

In this paper, electrical current systems external to Earth's surface are briefly reviewed. Effects that these current systems should be expected to have on field models produced from magnetic observatory monthly means are predicted (or hypothesized) based on symmetry arguments. First differences of magnetic observatory monthly means for 1963–1982 are analyzed using techniques of spherical harmonic analysis and power spectral analysis. Results of this analysis are compared with the predictions and are shown to be in good agreement. Except for Earth's auroral regions, the external source signal is shown to be primarily zonal in geomagnetic coordinates. The continuous spectrum is well represented by zonal degree 1 spherical harmonics. The continuous spectrum, with annual and semiannual spectral lines excluded, is used in this paper to estimate a global geomagnetic response function for periods ranging from 2 months to 2 years and sensitive to average radial electrical conductivity of the deep mantle down to the core-mantle boundary. The estimated response function found here agrees well with the response for the conductivity profile proposed by *Banks* [1969], as described by *Achache et al.* [1981], for which conductivity at the core-mantle boundary is about 10 S/m.

External Current Systems

Our knowledge of external current systems is based largely on observations from artificial Earth satellites and on magnetic observatory data. These current systems have been reviewed by *Potemra* [1991], *Russell and Luhmann* [1991], *McLeod* [1991], *Matsushita* [1967], and *Campbell et al.* [1989]. There are four major external current systems as described below. All of these current systems are modulated by solar activity.

A solar wind of ionized particles emanates continually from the Sun. This wind confines the geomagnetic field to a cavity that extends about 12 Earth radii from the center of Earth in the solar direction. The cavity extends over 1000 Earth radii from Earth's center in the antisolar direction, beyond the orbit of the Moon, and is about 30 Earth radii in diameter at Earth in the direction perpendicular to the solar direction. Dimensions of the cavity are mainly determined by pressure balance between solar wind pressure and pressure attributable to the geomagnetic field.

The cavity boundary is called the magnetopause. Electric currents flow on the magnetopause because the geomagnetic field deflects ionized solar wind particles; these currents produce a jump in magnetic field magnitude at the magnetopause. Field magnitude is nearly zero external to the cavity while field magnitude internal to the cavity is increased from what it would be if magnetopause currents were not present.

The jump in magnetic field magnitude at the magnetopause has been observed many times by spacecraft. Magnitude of the jump is typically about 50 nT but may be much greater when the magnetopause is close to Earth. Magnetopause location varies with solar wind pressure, so that a spacecraft moving away from Earth to interplanetary space may cross the magnetopause several times on a single trajectory as the magnetopause moves back and forth past the spacecraft. The magnetopause has been observed as close to Earth as 6.6 Earth radii [*Russell*, 1976]. Average solar wind pressure varies with sunspot activity; consequently, the portion of the average magnetic field at Earth's surface produced by magnetopause currents varies with the solar cycle, which has an approximate 11-year period.

A ring current is located at about 3.5 Earth radii from the center of Earth. The ring current encircles Earth near the plane of the geomagnetic equator. The current is due to ionized particles trapped in the geomagnetic field. Average ring current varies with solar activity and with the sunspot cycle.

The magnetic field produced by the ring current at Earth's surface is approximately in the opposite direction to the field produced by magnetopause currents. Both of these current systems are sufficiently far from Earth's surface that the field they produce can be well represented by degree 1 zonal spherical harmonics in geomagnetic coordinates.

Electric currents flow in the ionosphere at low latitudes and midlatitudes due mainly to tidal effects and to ionospheric heating by the Sun. Both mechanisms cause ionized particles to move in Earth's magnetic field; the field causes the charged particles to be deflected from what would otherwise be their trajectories, and the deflection of the charged particles gives rise to electric currents. Ionospheric current systems have been reviewed by *Matsushita* [1967] and *Campbell et al.* [1989]. The ionospheric current systems are approximately symmetric about the Sun-Earth line and about the geomagnetic equator at the times of the spring and fall equinoxes. These current systems consist largely of current loops centered near the noon meridian at about ±30° geomagnetic latitude at the times of the equinoxes and are

farther north or south at the times of the summer or winter solstices, respectively. As Earth rotates beneath these current systems, the magnetic field components at a fixed location on Earth's surface exhibit a time variation with a 1-day period. This time variation is called daily variation. Amplitude and waveforms of daily variation are different for different geomagnetic latitudes and seasons of the year and for different magnetic field components; a typical amplitude is ±30 nT.

Another external current system consists of currents that flow along magnetic field lines in Earth's magnetotail. The currents flow toward Earth on one side of the magnetotail and away from Earth on the other side of the magnetotail. These two current flows are connected by currents flowing in the ionosphere near auroral latitudes.

Expected Effects of External Current Systems on Magnetic Observatory Monthly Means

Because the magnetopause currents and the ring current are located far from Earth's center, they should be expected to produce a nearly uniform field, that is, a degree 1 field, over the entire surface of Earth. Because the ring current is caused by particles trapped in the geomagnetic field, which is primarily a dipole field at the location of the ring current, and because the magnetopause currents cancel Earth's dipole field external to the magnetosphere, both of these current systems should be expected to produce fields aligned with or opposed to Earth's dipole. A constant or DC component should be expected, and since solar activity varies with the sunspot cycle, harmonics of the sunspot cycle should also be expected. The size of the magnetosphere should be expected to vary seasonally as the strength of the dipole field at the subsolar point varies. The ring current also should be expected to vary seasonally as the angle between Earth's axis and the Sun-Earth line varies, since this could affect insertion of ionized particles into the ring current. There could also be an effect caused by seasonal variation of the solar latitude of Earth's orbital position. Symmetry considerations suggest that the seasonal variation should have a semiannual period and, in general, harmonics of that semiannual period. A continuous spectrum resulting from random variations in solar activity should be expected also.

Because the ionospheric current systems do not rotate with Earth but are approximately fixed in local time, daily averages of the field produced by these current systems should not be expected to have an east-west component. This is a consequence of Ampere's law for a potential field. Thus the average ionospheric source field should be approximately zonal in geomagnetic coordinates, provided the average is for an integral number of days and for a sufficiently long time. At the times of the equinoxes, symmetry considerations suggest that the field should have primarily odd-degree zonal spherical harmonics in geomagnetic coordinates, since Earth's dipole field is the principal field influencing these current systems.

Because the centers for the low-latitude and midlatitude ionospheric current systems at the times of the equinoxes are at ±30° geomagnetic latitude, a relatively large degree 3 spherical harmonic should be expected, together with a smaller degree 1 spherical harmonic and other odd-degree spherical harmonics. Since the centers for the current systems move north and south on a seasonal basis, zonal spherical harmonics of even degree should be expected at the times of the solstices; thus these even-degree spherical harmonics should vary with an annual period and odd harmonics of the annual period. The odd-degree spherical harmonics should vary with a semiannual period and its harmonics. Averaged over an entire year, the even-degree spherical harmonics should be zero, but the odd-degree spherical harmonics should not in general average to zero. Harmonics of the sunspot cycle and a constant or DC component should be expected for the odd-degree spherical harmonics. In general, a continuous spectrum due to random variations in solar activity should be expected as well. The preceding discussion is based on the fact that Earth's main field is approximately a dipole; however, since other spherical harmonics are small but significant at ionospheric altitudes, the ionospheric source field should be expected to be less nearly zonal than are the fields due to magnetopause currents or fields due to the ring current. The symmetry approximations are also less nearly exact at Earth's surface for the ionospheric source field than for the magnetopause source field or for the ring current field.

Data Set Selection

Data used in this study are magnetic observatory monthly means obtained from the National Geophysical Data Center (NGDC) operated by the National Oceanic and Atmospheric Administration (NOAA) of the U.S. Department of Commerce. The data were on a compact disk (CD-ROM) labeled NGDC01. The data set chosen for the study consisted of the monthly means of the vector field components from any magnetic observatory that had three-component vector data for any calendar month. The chosen monthly mean is an average for all days of the month and all times of day. Most of the analyses in this paper are for the 20-year time interval from 1963 to 1982, although a few illustrations are for the 60-year interval from 1923 to 1982. The observatories are not uniformly distributed about Earth; they are concentrated in Europe and Japan with relatively few located south of the geomagnetic equator, defined here as the equator for the geocentric magnetic dipole. The locations of the observatories are similar to those shown by *McLeod* [1992].

The selected data were lightly edited to reduce obvious errors. Time series for the first differences of the monthly means for each observatory were computed. The first differences for a given month at a given observatory were rejected if any first difference was greater than 200 nT/month. The lightly edited first difference time series were used for all further studies described here.

The data selection procedure described here for magnetic observatory monthly means is similar to that for annual means described by *McLeod* [1992]. Most of the analyses in this study are for nearly the same time interval used in the previous study, 1961–1983. Figure 1 shows the number of observatories with available first differences of monthly means for each month in the time interval 1920–1990. The number of available observatories for each month in the 1963–1982 portion of this study varied from 29 to 113, with a typical value of 45; in contrast, the same set of 73 observatories was used for each individual year in the previous study.

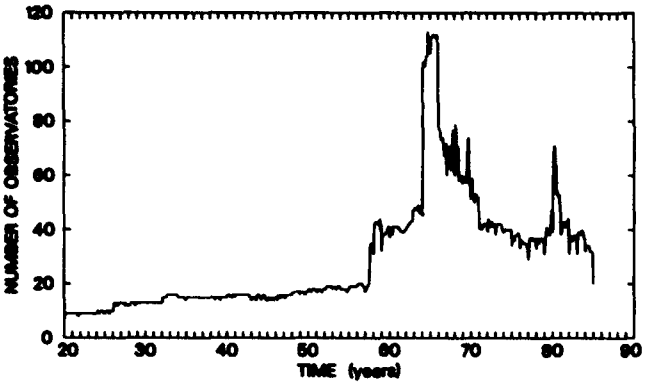

Figure 1. Available magnetic observatory monthly means. The number of observatories with available first differences of monthly means is shown for each individual month in the time interval 1920–1990.

Data Analysis

Spherical harmonic coefficients in geomagnetic coordinates were computed for first differences of magnetic observatory monthly means from the selected data set using a weighted least squares procedure. Fourier series for individual spherical harmonic coefficients were then determined and used to compute periodograms, power spectra, and cross spectra. The analysis procedure is described in greater detail in the following sections.

Spherical Harmonic Analysis

The method of spherical harmonic analysis used in this study was the same as that used by *McLeod* [1992]. The geomagnetic field vector first differences and observatory locations were transformed to a geomagnetic coordinate system. Geomagnetic coordinates are defined by a rotation of the geocentric coordinate system such that the axis of the geomagnetic coordinate system coincides with the axis of Earth's magnetic dipole.

Spherical harmonic models of the first differences of the magnetic observatory monthly means were constructed. It is very important to the analysis that the first differences be computed before the spherical harmonic analysis is performed, in contrast to first performing the spherical harmonic analysis on the monthly means and then computing first differences of the spherical harmonic coefficients. To understand this, consider that the observatory monthly means contain nearly constant crustal source fields. When first differences are calculated first, the effects of a constant bias in the monthly means is eliminated, so that the crustal source fields have almost no effect on the computed first difference spherical harmonic coefficients. If the spherical harmonic analysis had been performed first, the crustal source fields would produce spatial aliasing errors. Since not every observatory is used for the full time interval selected for study, the aliasing errors would have discontinuities at the times when data from a particular observatory begins or ends. These discontinuities would cause errors in the computed first differences of the spherical harmonic coefficients. The same principle that applies to crustal source aliasing errors applies to low-frequency spatial aliasing errors from unmodeled core source spherical harmonics. That is, the aliasing errors are larger and are shifted upward in temporal frequency if the spherical harmonic analysis is done first, since not every observatory has data for the entire time interval selected for study.

Errors for each field component at each observatory were estimated using the procedure described by *McLeod* [1992]. Third differences of the measured monthly means were computed for each field component at each observatory. Third differences computed from a model field were subtracted from the measured third differences to obtain residual third differences. The rms residuals were assumed to be good indicators of data quality, for reasons stated by *McLeod* [1992], and were used as weights for the weighted least squares computation of spherical harmonic models used in this study.

The rms residuals are believed to be mostly noise and auroral ionospheric source geomagnetic signals of spherical harmonic degrees that are too large to be modeled with available observatory monthly means. Residuals were large for auroral zone observatories, so data from these observatories had little effect on the computed models.

Spectral Analysis

Spherical harmonic coefficients for first differences of monthly means for the 20-year time interval 1963–1982 were spectrally analyzed. Power at each Fourier frequency for each coefficient was determined. The Fourier frequencies are multiples of the fundamental frequency, 0.05 cycle per year (c/yr) from 0.00 c/yr to the Nyquist frequency, 6.00 c/yr. This set of spectral estimates is sometimes called a periodogram; each estimate has 2 degrees of freedom.

Power was computed for four different frequency bands: (1) a low-frequency band from 0.000 to 0.125 c/yr for which power was found by summing the power for Fourier frequencies 0.00, 0.05, and 0.10 c/yr; (2) an annual frequency band from 0.925 to 1.075 c/yr for which power was found by summing the power for Fourier frequencies 0.95, 1.00, and 1.05 c/yr; (3) a semiannual frequency band from 1.925 to 2.075 c/yr for which power was found by summing the power for Fourier frequencies 1.95, 2.00, and 2.05 c/yr; and (4) a band consisting of all other frequencies for which power was found by subtracting the power for the previous three frequency bands from the total power. The band limits given are approximations; the frequency window for a periodogram has sidelobes, as discussed by *Marple* [1987], but the frequency window is approximated here as a rectangular window with boundaries midway to the adjacent Fourier frequencies.

Spectra and cross spectra were estimated for zonal degree 1 coefficients. Spectra were estimated from the periodograms by averaging over frequency; the power for a given Fourier frequency was estimated as the average of the periodogram power for that frequency and the five adjacent Fourier frequencies on each side of the given Fourier frequency. This method of spectral estimation, called the Wiener-Daniell method, is discussed in many texts including *Otnes and Enochson* [1978], *Marple* [1987], and *Gardner* [1988]. The method was chosen because of its simplicity and because of its relatively small frequency window sidelobes in comparison to some other methods, such as the Bartlett method or the classic Blackman-Tukey method. Each spectral estimate has 22 degrees of freedom; therefore the

Table 1a. Variances for All Frequencies From 0.000 to 6.000 c/yr of Spherical Harmonic Coefficients for First Differences of Magnetic Observatory Monthly Means

N	M	G	H	Q	S
1	0	25.710		56.393	
1	1	6.950	4.290	3.389	2.867
2	0	12.560		5.692	
2	1	9.433	5.141	3.508	4.519
2	2	4.642	15.312	3.521	3.690
3	0	2.972		3.643	
3	1	2.388	4.159	1.615	1.828
3	2	3.071	2.614	2.398	1.402
3	3	2.115	4.271	1.477	2.785

N and *M* are the degree and order of the coefficients, *G* and *H* are internal coefficients, and *Q* and *S* are external coefficients. Variances are mean square first difference fields associated with each coefficient in units of $(nT/mo)^2$.

Table 2a. Variances for Annual Frequency Band From 0.925 to 1.075 c/yr of Spherical Harmonic Coefficients for First Differences of Magnetic Observatory Monthly Means

N	M	G	H	Q	S
1	0	0.072		0.260	
1	1	0.072	0.077	0.050	0.173
2	0	0.148		2.931	
2	1	0.024	0.100	0.404	0.591
2	2	0.034	0.131	0.081	0.251
3	0	0.037		0.019	
3	1	0.024	0.051	0.046	0.062
3	2	0.029	0.045	0.070	0.157
3	3	0.060	0.147	0.139	0.113

N and *M* are the degree and order of the coefficients, *G* and *H* are internal coefficients, and *Q* and *S* are external coefficients. Variances are mean square first difference fields associated with each coefficient in units of $(nT/mo)^2$.

standard deviation of a spectral estimate is 30% of the power spectral density for the frequency corresponding to that spectral estimate. It is assumed that the underlying random process is stationary, Gaussian, and ergodic and that the spectrum is flat over the range of frequencies used for the spectral estimate. Since these assumptions may not be valid, the stated standard deviation may be less than the true standard deviation. Low-frequency, annual, and semiannual frequency bands were removed from the periodograms before computing estimated spectra by setting the power equal to zero for Fourier frequencies 0.00, 0.05, 1.00, 1.95, 2.00, and 2.05 c/yr. In order to compute spectral estimates near the ends of the frequency range, it was assumed that the periodograms are symmetric about the origin and Nyquist frequency.

Cross spectra between internal and external zonal degree 1 spherical harmonic coefficients were computed in a similar manner. The real part of the cross spectrum was assumed to be symmetric, and the imaginary part of the cross spectrum was assumed to be antisymmetric, about the origin and Nyquist frequency.

Let S_e and S_i be the power spectral density estimates for the external and internal zonal degree 1 spherical harmonic coefficients, and let C be the cross-spectral estimate for these coefficients. If the coefficients can be related by a transfer function T, an estimated value of T can be found from

$$T = C/S_e. \tag{1}$$

The correlation R is defined by

$$R^2 = (CC^*)/(S_iS_e), \tag{2}$$

where the asterisk stands for complex conjugate. The standard deviation σ_T for the magnitude of T, $(TT^*)^{1/2}$, is

$$\sigma_T/T = 0.30(1 - R^2)^{1/2}, \tag{3}$$

where the cross-spectral estimate is assumed to have 22 degrees of freedom.

Equation (3) yields an estimate of the error in the direction of the complex vector T. Assuming that the estimated error in the direction perpendicular to T has the same value, the error in phase angle and in the real and imaginary parts of T can be found.

Spatial and Temporal Spectra

Tables 1 and 2 show mean square values (variances) of geomagnetic field first differences associated with each spherical harmonic coefficient in geomagnetic coordinates for model 3/3 W. This model is of degree and order 3 for both internal source and external source terms. Parameters *G* and *H* are internal source spherical harmonic coefficients, while *Q* and *S* are external source spherical harmonic coefficients, as described by *McLeod* [1992]. Parameters *N* and *M* are degree and order, respectively, for the coefficients; those coefficients for which $M = 0$ are called zonal coefficients. Variances are shown for four different frequency bands. The first difference field variances were computed from the

Table 1b. Variances for Low Frequencies From 0.000 to 0.125 c/yr

N	M	G	H	Q	S
1	0	14.336		0.456	
1	1	3.196	0.134	1.307	0.094
2	0	10.109		0.286	
2	1	7.626	1.859	1.362	0.611
2	2	0.885	10.778	0.128	0.467
3	0	1.110		0.278	
3	1	1.428	3.056	0.535	0.252
3	2	0.927	1.053	0.082	0.129
3	3	0.997	1.779	0.419	0.141

See Table 1a footnotes.

Table 2b. Variances for Semiannual Frequency Band From 1.925 to 2.075 c/yr

N	M	G	H	Q	S
1	0	1.368		4.657	
1	1	0.101	0.207	0.054	0.176
2	0	0.156		0.235	
2	1	0.092	0.120	0.058	0.099
2	2	0.058	0.123	0.175	0.061
3	0	0.176		1.430	
3	1	0.020	0.070	0.099	0.331
3	2	0.013	0.051	0.193	0.018
3	3	0.038	0.099	0.018	0.168

See Table 2a footnotes.

Table 2c. Variances for Frequencies From 0.000 to 6.000 c/yr With Variances for the Low, Annual, and Semiannual Frequency Bands Removed

N	M	G	H	Q	S
1	0	9.934		51.019	
1	1	3.582	3.872	1.978	2.424
2	0	2.147		2.241	
2	1	1.691	3.063	1.684	3.217
2	2	3.666	4.281	3.138	2.912
3	0	1.648		1.916	
3	1	0.917	0.982	0.935	1.183
3	2	2.102	1.465	2.053	1.098
3	3	1.020	2.246	0.901	2.363

See Table 2a footnotes.

spherical harmonic coefficients using formulas given by *Lowes* [1966], valid for the Schmidt seminormalized spherical harmonic representation.

Table 1 shows variances for all frequencies up to the Nyquist frequency and for the low-frequency band. Except for the degree 1 zonal terms, variances for low frequencies represent a major portion of the variances for all frequencies. The internal source coefficients for low frequencies agree fairly well with values computed for annual means by *McLeod* [1992]. It will be shown that the external source coefficients for low frequencies are mostly due to spatial aliasing from unmodeled internal source coefficients.

Table 2 shows variances for annual and semiannual frequency bands and a band which extends from zero frequency to the Nyquist frequency with the low, annual, and semiannual bands removed. The annual frequency component is largest by far for the external zonal spherical harmonic of degree 2; however, two other external spherical harmonics of degree 2 are also significantly larger than the remaining spherical harmonics. The semiannual frequency component is largest for the zonal degree 1 spherical harmonics and for the external zonal degree 3 spherical harmonic. The band which consists of all frequencies up to the Nyquist frequency, with low, annual, and semiannual bands removed, is largest for the zonal degree 1 spherical harmonics. This band will be called the continuous spectrum in the remainder of this article. The variances of Table 2 are in good general agreement with the predictions (or hypotheses) made earlier.

Table 3 is the same as Table 2 except that it is for model 3/3Z W (which has 20 parameters) in contrast to model 3/3 W of Table 2 (which has 30 parameters). All variances for the continuous spectrum except for the zonal degree 1 harmonics are significantly smaller for Table 3 than for Table 2. This result is consistent with the interpretation that the variances shown in Table 2 for these spherical harmonics of the continuous spectrum are mostly due to noise or spatial aliasing from unmodeled harmonics. The external zonal variances and internal degree 1 zonal variances for the annual and semiannual frequency components differ appreciably between Tables 3 and 2. This finding is consistent with the interpretation that spatial aliasing errors from unmodeled spherical harmonics for these frequency components are responsible for the differences between the two models. In contrast, the zonal degree 1 variances for the continuous spectrum are nearly the same for the two models. Therefore the continuous spectrum should be more useful than the annual or semiannual lines for analysis of deep mantle conductivity, since the continuous spectrum is less subject to spatial aliasing errors. All these results are consistent with the interpretation that ionospheric current systems make a relatively larger contribution to the annual and semiannual frequency components than to the continuous spectrum.

Figure 2 shows rms field derivatives for the external degree 1, 2, and 3 spherical harmonics for model 3/3Z W. The rms values for the field derivatives were computed from the spherical harmonic coefficients using the formulas of *Lowes* [1966]. The graphs are plots against time of the individual spherical harmonic coefficients multiplied by an $n^{1/2}$ scale factor, where n is the spherical harmonic degree. The annual frequency component is evident on the graph for the degree 2 coefficient, and the semiannual component is evident on the graph for the degree 3 coefficient.

Table 3a. Variances for Annual Frequency Band From 0.925 to 1.075 c/yr of Spherical Harmonic Coefficients for First Differences of Magnetic Observatory Monthly Means

N	M	G	H	Q	S
1	0	0.052		0.215	
1	1	0.146	0.126	0.333	0.052
2	0	0.156		2.890	
2	1	0.032	0.062		
2	2	0.010	0.016		
3	0	0.119		0.060	
3	1	0.033	0.014		
3	2	0.037	0.020		
3	3	0.022	0.028		

See Table 2a footnotes. The model used for this table has fewer parameters than the model used for Table 2.

Table 3b. Variances for Semiannual Frequency Band From 1.925 to 2.075 c/yr

N	M	G	H	Q	S
1	0	1.828		5.441	
1	1	0.138	0.072	0.111	0.035
2	0	0.076		0.124	
2	1	0.129	0.010		
2	2	0.011	0.034		
3	0	0.065		0.879	
3	1	0.033	0.017		
3	2	0.017	0.045		
3	3	0.017	0.028		

See Table 3a footnotes.

Table 3c. Variances for Frequencies From 0.000 to 6.000 c/yr With Variances for the Low, Annual, and Semiannual Frequency Bands Removed

N	M	G	H	Q	S
1	0	9.164		50.706	
1	1	1.540	1.382	0.615	0.872
2	0	1.283		1.154	
2	1	0.725	0.965		
2	2	1.421	0.799		
3	0	0.759		1.015	
3	1	0.531	0.497		
3	2	0.827	0.534		
3	3	0.392	0.833		

See Table 3a footnotes.

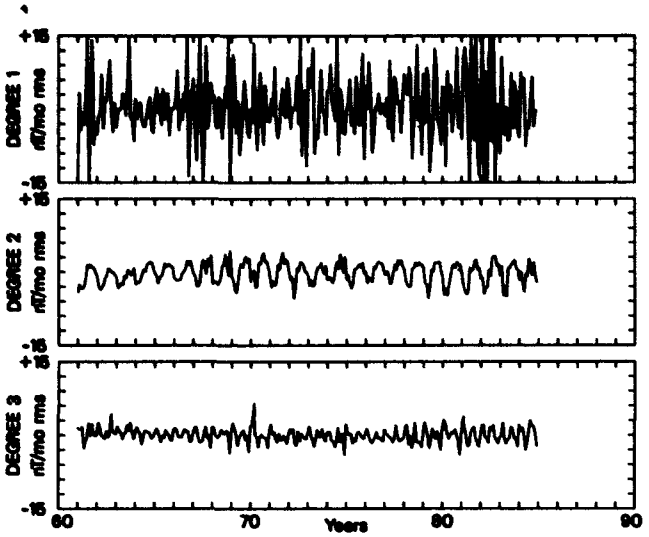

Figure 2. External field derivatives for various spherical harmonic degrees. Global rms first differences for zonal degree 1, 2, and 3 external spherical harmonics are plotted against time for the time interval 1960–1990. A geomagnetic coordinate system is used. The graphs are for model 3/3Z W.

Figure 3 shows periodograms for the functions shown in the graphs of Figure 2. The annual and semiannual lines are evident in addition to the degree 1 continuous spectrum.

Figures 4 and 5 show amplitude and phase of the annual and semiannual lines in the external zonal degree 1, 2, and 3 spherical harmonics. The spherical harmonic coefficients are multiplied by $n^{1/2}$ as for Figures 2 and 3 to obtain global rms field derivatives. Figure 4 is for model 3/3Z W, which was used for Figures 2 and 3. Figure 5 is for a longer time interval than Figure 4 and is for model 1Z/3Z W, which has only four parameters, namely, zonal degree 1 internal and external coefficients and zonal degree 2 and 3 external coefficients. Fewer parameters were used for the longer time interval because there are fewer observatories with available monthly means for the earlier years as shown in Figure 1.

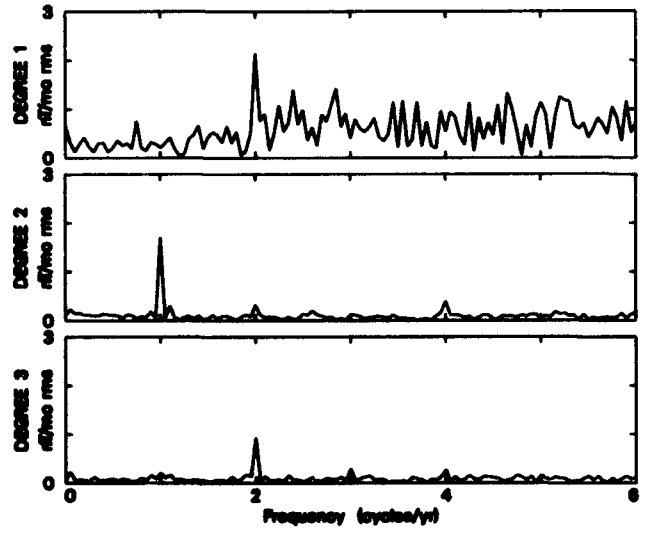

Figure 3. Periodograms for external field derivatives for various spherical harmonic degrees. These are periodograms for the time series plotted in Figure 2.

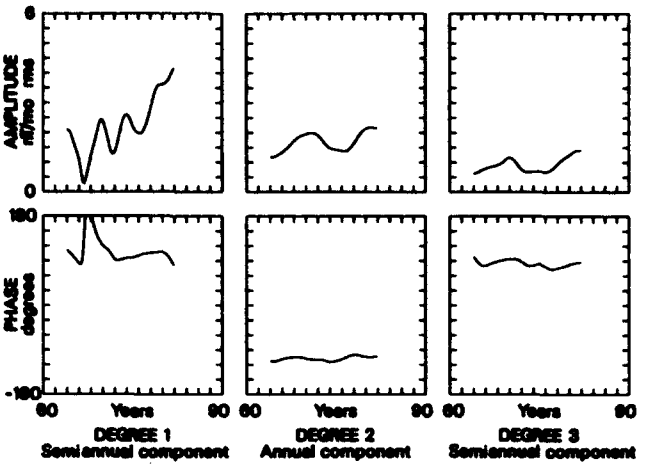

Figure 4. Amplitude and phase plotted against time for annual and semiannual spectral lines in external field derivatives. The graphs are for zonal external degree 1, 2, and 3 spherical harmonics for the time series plotted in Figure 2.

Amplitude and phase for a particular time were computed from corresponding Fourier series coefficients for a 2-year interval centered on the particular time. These coefficients for the annual and semiannual lines were then filtered twice using a 2-year running average before computing amplitude and phase. Phase is measured relative to the beginning of the calendar year so that the phase is zero if the annual or semiannual line has maxima at the beginning of the calendar year. Figures 4 and 5 are very similar for the time period that they overlap.

Figure 6, taken from *McLeod* [1991], shows sunspot number and its first derivative plotted against time. The zonal degree 1 external field and its first derivative are also shown plotted against time. The field derivative was computed from magnetic observatory annual means by the method of stochastic inversion as discussed by *McLeod* [1991]. The a priori error covariance matrix for the inversion was determined using the method of *McLeod* [1992] and the

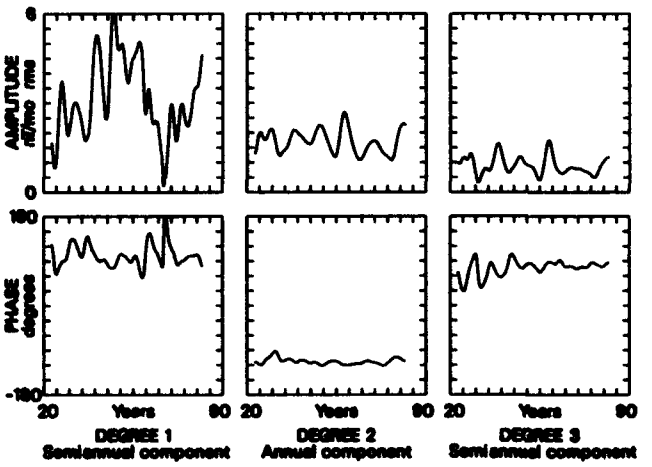

Figure 5. Amplitude and phase plotted against time for annual and semiannual spectral lines in external field derivatives. Same as Figure 4 except that it is for a longer time interval and for model 1Z/3Z W which has only four parameters.

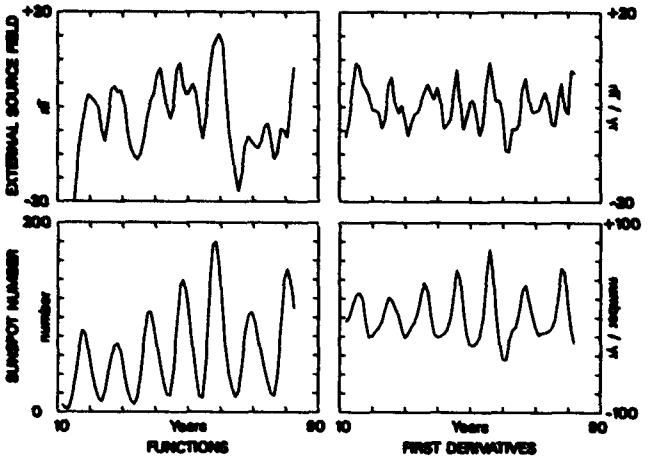

Figure 6. Sunspot number and external zonal degree-one spherical harmonic coefficient for geomagnetic field plotted against time. Derivatives of these functions are also shown. The time series have been filtered as discussed in the text. A geomagnetic coordinate system is used. This figure is from *McLeod* [1991].

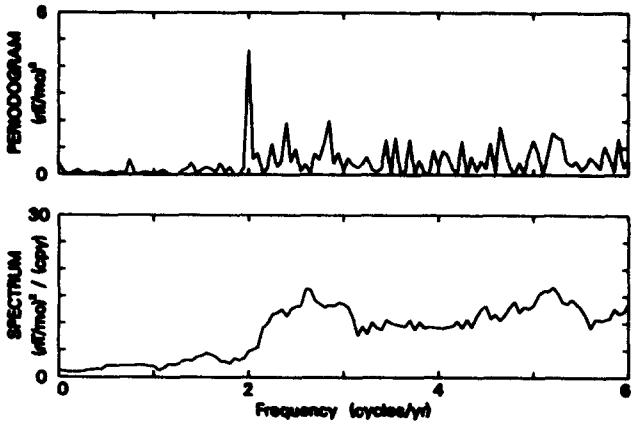

Figure 7. Periodogram and spectrum for first differences of external zonal degree 1 spherical harmonic. The spectrum is computed from the periodogram by averaging over frequency after removing annual and semiannual spectral lines. The same model 3/3Z W was used as was used for Figure 3.

a priori parameter covariance matrix for the inversion was estimated from models given by *McLeod* [1992]. Both matrices were assumed to be diagonal, and the parameter covariances were assumed to depend on spherical harmonic degree but not order. The field was obtained by digital integration of the field derivative with mean removed; therefore the mean values of the field and its derivative were not determined and are shown as zero in Figure 6. All waveforms shown in Figure 6 have been filtered with weights (0.25, 0.50, 0.25); this filter has a frequency response similar to the filter used for Figure 5.

The amplitude waveform for the external zonal degree 1 semiannual line shown in Figure 5 is similar to the field waveform for the external zonal degree 1 harmonic shown in Figure 6; both of these waveforms are correlated with the sunspot number waveform shown in Figure 6. The degree 2 annual line and the degree 3 semiannual line amplitude waveforms shown in Figure 5 are very similar to each other and are correlated with sunspot number. The degree 2 and 3 waveforms are believed to be due to ionospheric currents for reasons previously discussed; the time variation of these waveforms may reflect time variation of ionization in the ionosphere.

Figure 7 shows a periodogram and spectrum for the external zonal degree 1 harmonic for model 3/3Z W. The spectrum is the average over frequency of the periodogram and has 22 degrees of freedom. Low-frequency, annual, and semiannual frequency bands were removed from the periodogram before computing the spectrum. The spectrum is approximately white but has less power at frequencies below 2 c/yr than above this frequency.

Figure 8 shows amplitude and phase of the transfer function between zonal internal and external degree 1 spherical harmonic coefficients computed for model 3/3Z W. The computed correlation for the cross spectrum is also shown in Figure 8.

Figure 9 is the same as Figure 8 except that Figure 9 is for model 5Z/5Z W, which has only 10 parameters (the zonal internal and external coefficients through degree 5), in contrast to model 3/3Z W, which has 20 parameters and which was used for Figure 8. The correlation is generally higher and the graph of transfer function phase against frequency is smoother for the model with fewer parameters shown in Figure 9. The transfer function is useful for determining deep mantle conductivity, as will be discussed in the next section.

Figure 10 shows graphs of first differences of magnetic observatory monthly mean field components for the Hartland, England, magnetic observatory. The measured monthly mean first differences are shown together with first differences for the internal source and external source monthly mean field computed from model 3/3Z W. Residuals to the model are shown in the figures; the residuals are the difference between model first differences and measured first differences. The model fits the measurements well at this

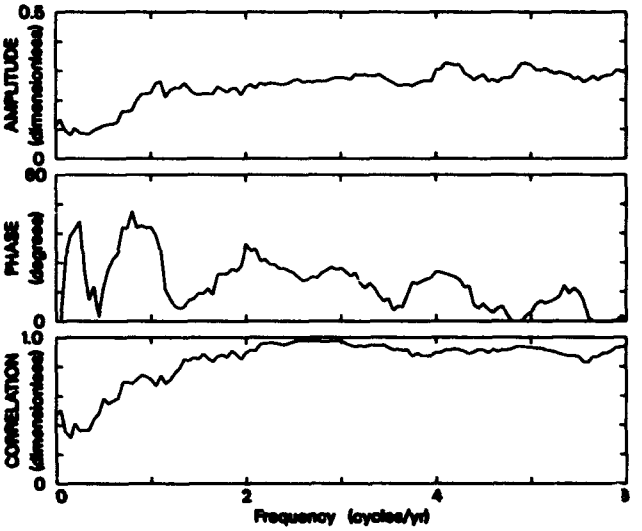

Figure 8. Transfer function between zonal internal degree 1 induced field and zonal external degree 1 inducing field. Amplitude and phase of the transfer function computed for model 3/3Z W are plotted against frequency. Computed correlation between the zonal degree 1 spherical harmonic coefficients is also plotted against frequency.

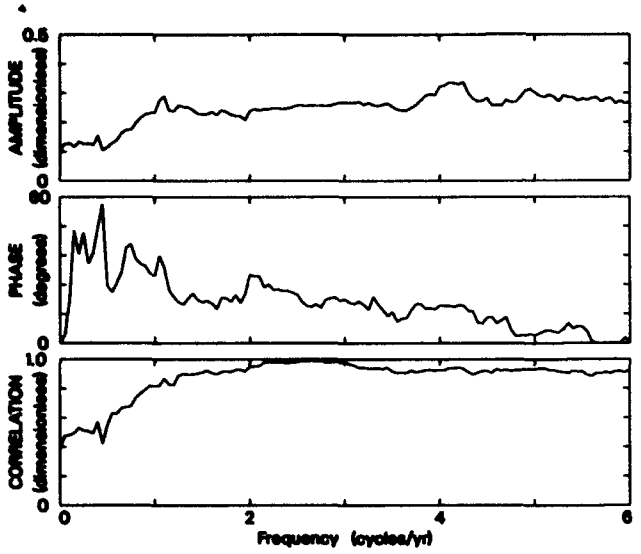

Figure 9. Transfer function between zonal internal degree 1 induced field and zonal external degree 1 inducing field. This figure is the same as Figure 8 except that it is for model 5Z/5Z W which has only 10 parameters.

observatory. The model is found to be generally poor at high-latitude observatories but good at midlatitude and low-latitude observatories.

The vertical magnetic field first differences shown in Figure 10 for the Hartland, England, magnetic observatory exhibit a pair of outlying points at approximately 1983.5 in both measured data and residuals. These outliers are due to a single outlier at approximately 1983.5 in the vertical monthly means for Hartland. This single outlier produces an outlier pair in the first differences of the monthly means. Similar outlier pairs are evident in graphs for other magnetic observatories (not shown) and are believed due to clerical error in compiling the data sets. Similar outliers were found in the annual mean data set used by *McLeod* [1992].

An edited first difference data set was created from the lightly edited first difference data set. This edited data set was obtained by deleting all first differences from a given observatory for any month in which any of the first differences for that observatory were judged to be outliers. Also, data from a few observatories were eliminated because those observatories had data for only a few months. About 3% of the first difference data were deleted in this manner to obtain the edited first difference data set. The letter E is used in a model name to indicate that the model was computed from the edited data set.

Table 4 is the same as Table 3 except that Table 4 is for model 3/3Z WE and Table 3 is for model 3/3Z W. All variances for the continuous spectrum of Table 4 are less than corresponding variances of Table 3, except for the zonal degree 1 variances. This observation is consistent with the interpretation that the continuous spectrum variances of Table 3, except for zonal degree 1 variances, are mostly due to noise in the data set caused by outliers; this noise is reduced through use of the edited data set.

A graph similar to Figure 9 was produced, except that the transfer function was computed using the edited data set in place of the lightly edited data set used for Figure 9. The correlation function is generally closer to unity for the edited data than for the lightly edited data.

To reduce errors due to spatial aliasing by unmodeled coefficients in the spherical harmonic analysis of first differences of magnetic observatory monthly means, a reference model for first differences of monthly means was created. This reference model was created from the internal source

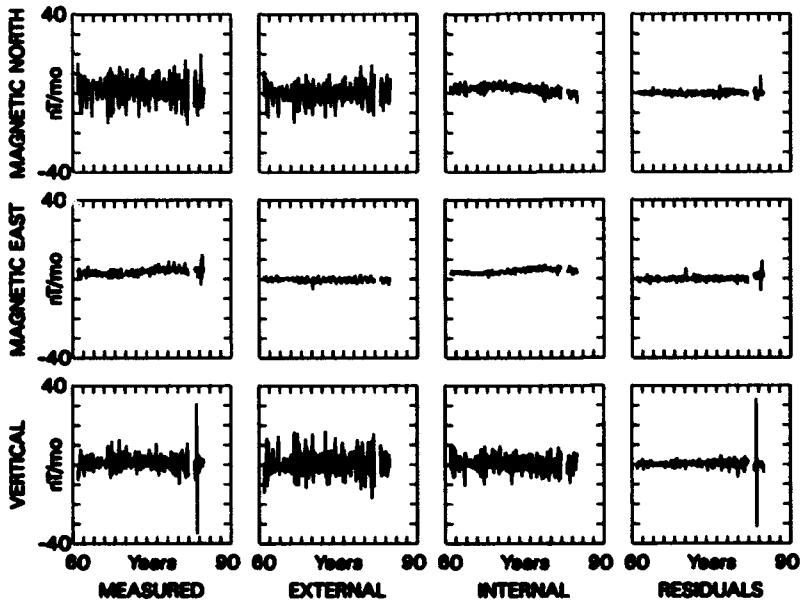

Figure 10. First differences of Hartland, England, magnetic observatory monthly mean field components. Measured first differences for three field components are shown together with first differences of external source and internal source monthly mean field computed from model 3/3Z W. Residuals to the model are also shown; the residuals are the difference between model first differences and measured first differences.

Table 4a. Variances for Annual Frequency Band From 0.925 to 1.075 c/yr of Spherical Harmonic Coefficients for First Differences of Magnetic Observatory Monthly Means

N	M	G	H	Q	S
1	0	0.047		0.307	
1	1	0.198	0.158	0.304	0.039
2	0	0.135		2.861	
2	1	0.059	0.118		
2	2	0.028	0.016		
3	0	0.116		0.035	
3	1	0.026	0.009		
3	2	0.048	0.017		
3	3	0.027	0.025		

See Table 3a footnotes. The model used for this table is based on edited data as described in the text.

Table 4c. Variances for Frequencies From 0.000 to 6.000 c/yr With Variances for the Low, Annual, and Semiannual Frequency Bands Removed

N	M	G	H	Q	S
1	0	8.996		51.294	
1	1	0.987	0.956	0.499	0.512
2	0	0.836		0.968	
2	1	0.563	0.590		
2	2	0.828	0.512		
3	0	0.589		0.759	
3	1	0.359	0.345		
3	2	0.487	0.336		
3	3	0.289	0.477		

See Table 4a footnotes.

portion of model 7/7Z W for first differences of annual means described by *McLeod* [1992]. The annual means first difference coefficients were filtered with weights (0.25, 0.50, 0.25) and used to compute filtered first difference coefficients for monthly means by means of parabolic interpolation. First differences for the reference model were subtracted from the magnetic observatory first differences; spherical harmonic coefficients for the first difference residuals were then computed. The coefficients for the first difference residuals were then added to the coefficients for the reference field to obtain coefficients for the monthly means. The model for the first difference residuals was not generally of the same degree and order as the reference model. When this method of analysis is used, the coefficients of the reference model that are also included in the residual model have no effect on the final result. This is because a change in these coefficients of the reference model produces a corresponding change in the residual model, so that the final sum model is unchanged. However, the coefficients of the reference model that are not included in the residual model can have a large effect on the final model.

A model of degree and order 3 for both internal and external spherical harmonics, model 3/3 WER, was produced from the edited data set using the reference model. Variances were computed for this model and compared with those shown in Tables 1 and 2. It was found that external coefficient variances for the low-frequency band shown in Table 1b were greatly reduced for the new model. It was concluded that these external variances in Table 1b are mostly due to spatial aliasing by unmodeled internal coefficients and that this aliasing is greatly reduced by using the reference model. Variances for the continuous spectrum shown in Table 2c, except for the zonal degree 1 harmonics, were also reduced for the new model.

Additional models with various combinations of internal and external coefficient were produced. An expanded version of this article that includes spectra and cross spectra for these models is available from the author. It was found that the best model for determining a transfer function between internal and external zonal degree 1 spherical harmonic coefficients was model 1Z/3Z WER. Variances for this model are shown in Table 5. The transfer function is shown in Figure 11. This model was considered best for determining a transfer function, since the correlation shown in Figure 11 was generally closer to unity for this model than for other models. Variances for the continuous spectrum, except for the zonal degree 1 harmonics, were generally smaller for this model than the other models.

Table 4b. Variances for Semiannual Frequency Band From 1.925 to 2.075 c/yr

N	M	G	H	Q	S
1	0	1.785		5.706	
1	1	0.098	0.093	0.125	0.019
2	0	0.027		0.124	
2	1	0.078	0.003		
2	2	0.010	0.025		
3	0	0.062		0.800	
3	1	0.038	0.020		
3	2	0.019	0.024		
3	3	0.008	0.026		

See Table 4a footnotes.

Deep Mantle Conductivity

Time-varying magnetic fields that originate from electrical current systems external to Earth induce electrical currents within Earth. These induced currents in turn produce time-varying magnetic fields. The transfer function between induced and inducing spherical harmonic coefficients for a given degree spherical harmonic can be used to study electrical conductivity of Earth as a function of depth. Lateral homogeneity is assumed here as a reasonable approximation so that the transfer function depends upon the degree but not the order of the spherical harmonic. The transfer function also depends upon temporal frequency and upon the conductivity profile of Earth.

If Earth is assumed to be an insulator for $r > b$ and an ideal conductor for $r < b$, then the transfer function between induced and inducing spherical harmonic coefficients is easily found from the boundary condition that the vertical field must be zero within the conductor. The transfer function $T_n(\omega)$ for Schmidt seminormalized spherical harmonic coefficients is found to be

$$T_n(\omega) = \frac{n}{n+1}(b/a)^{2n+1}, \tag{4}$$

where n is the spherical harmonic degree, $\omega = 2\pi f$, f is temporal frequency, and a is Earth's radius.

Induction only by degree 1 spherical harmonics will be considered in this section, and the transfer function will

Table 5a. Variances for Annual Frequency Band From 0.925 to 1.075 c/yr of Spherical Harmonic Coefficients for First Differences of Magnetic Observatory Monthly Means

N	M	G	H	Q	S
1	0	0.039		0.265	
2	0			2.536	
3	0			0.032	

See Table 3a footnotes. The model used for this table is based on a reference field and edited data as described in the text.

Table 5c. Frequencies From 0.000 to 6.000 c/yr With Variances for the Low, Annual, and Semiannual Frequency Bands Removed

N	M	G	H	Q	S
1	0	8.548		52.580	
2	0			0.552	
3	0			0.610	

See Table 5a footnotes.

simply be called $T(\omega)$. Assume that the mantle acts as an insulator and the core acts as an ideal conductor as ω approaches zero. For a core radius c equal to 3485 km and an Earth radius a equal to 6371 km, equation (4) yields

$$\lim_{\omega \to 0} T(\omega) = 0.0818. \tag{5}$$

Some authors, such as *Constable* [1993], define a transfer function $W(\omega)$ which is related to $T(\omega)$ by

$$W(\omega) = [1 - 2T(\omega)]/[1 + T(\omega)] \tag{6}$$

and define a complex admittance $c(\omega)$ which is related to $W(\omega)$ by

$$c(\omega) = (a/2)W(\omega) \tag{7}$$

where a is Earth's radius. If $T(\omega)$ is given by (4) for $n = 1$, then $c(\omega)$ is approximately the penetration depth provided that $(a - b) \ll a$.

Table 6 shows measured values of the magnitude and phase of the transfer function T for model 1Z/3Z WER at eight different frequencies. This is the transfer function shown in Figure 11. This transfer function is thought to be the best estimate for T, since the computed correlation function is generally closer to unity for this model than for other models considered in this article. Computed correlation function R is also tabulated. The measured values are nearly statistically independent for the different frequencies, since these measured values are averages over 11 Fourier frequencies and adjacent measured values have only a single Fourier frequency in common. The real and imaginary components of the transfer function T are tabulated with the estimated error in these components. The real and imaginary parts of transfer function W and complex admittance c, as well as estimated errors for these quantities, are also shown in Table 6.

Values of the transfer function T from Table 6 are plotted against period in Figure 12. The real part of T from Table 6 is shown as solid squares, and the imaginary part of T from Table 6 is shown as open squares. Values of the complex admittance c from Table 1 of the article by *Constable* [1993] were used to compute corresponding values of T which are also plotted in Figure 12. The real part of T from *Constable* [1993] is shown as solid circles, and the imaginary part of T from *Constable* [1993] is shown as open circles. Formal error estimates for T from Table 6 and computed from error estimates given by *Constable* [1993] are shown as error bars. Figure 12 shows that the estimates of T from Table 6 are in good agreement with the estimates given by *Constable* [1993] for the small range of periods where the estimates overlap.

A transfer function $T(s)$ given by

$$T(s) = 0.0818[(1 + sA)(1 + sB)(1 + sC)] \div [(1 + sD)(1 + sE)(1 + sF)] \tag{8}$$

was fit to the data shown in Figure 12, using a weighted least squares procedure. The variable $s = i\omega$ is the Laplace transform variable while i is the imaginary square root of -1. The value of $T(s)$ for $s = i\infty$ was constrained to the value 0.3602 which corresponds to an insulating mantle above a depth of 660 km. This transfer function was chosen because it has the desired asymptotic behavior for $s = 0$ and $s = i\infty$, and because positive values for the real parts of parameters

Table 5b. Variances for Semiannual Frequency Band From 1.925 to 2.075 c/yr

N	M	G	H	Q	S
1	0	1.945		6.492	
2	0			0.173	
3	0			0.638	

See Table 5a footnotes.

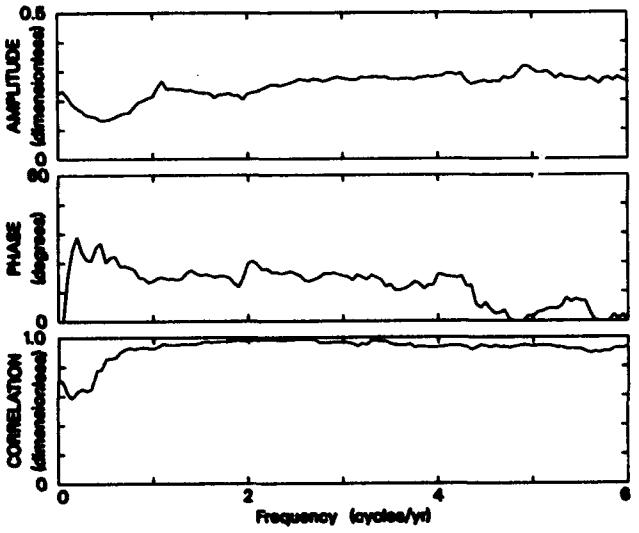

Figure 11. Transfer function between zonal internal degree 1 induced field and zonal external degree 1 inducing field. This figure is the same as Figure 8 except that it is for model 1Z/3Z WER which has only four parameters and which was computed from more heavily edited data using a reference field. See text for details.

Table 6. Global Geomagnetic Response Functions for Spherical Harmonic Degree 1

Number	Frequency, c/yr	Period, s	Correlation	Magnitude (T)	Phase (T), deg	Real (T)	Imaginary (T)	Error (T)	Real (W)	Imaginary (W)	Error (W)	Real (c), km	Imaginary (c), km	Error (c), km
1	0.5	63115200	0.854	0.133	24.21	0.121	0.055	0.021	0.669	−0.130	0.049	2132	−414	157
2	1.0	31557600	0.923	0.213	16.44	0.204	0.060	0.025	0.485	−0.124	0.051	1545	−396	162
3	1.5	21038400	0.964	0.227	18.67	0.215	0.073	0.018	0.460	−0.147	0.037	1466	−469	117
4	2.0	15778800	0.979	0.223	23.93	0.204	0.090	0.014	0.478	−0.186	0.028	1523	−593	89
5	2.5	12623040	0.987	0.266	19.51	0.251	0.089	0.013	0.387	−0.169	0.024	1231	−540	78
6	3.0	10519200	0.968	0.276	18.58	0.262	0.088	0.021	0.366	−0.165	0.039	1167	−526	124
7	3.5	9016457	0.955	0.273	15.05	0.264	0.071	0.024	0.367	−0.133	0. .5	1168	−423	145
8	4.0	7889400	0.934	0.283	19.21	0.267	0.093	0.030	0.355	−0.173	0.056	1130	−551	180

Estimated values of the transfer functions T, W, and c (as defined in text) are given for various frequencies (in cycles per year) and periods (in seconds). Magnitude and phase of transfer function T, as determined from spectral and cross-spectral estimates for monthly means during the interval 1963–1982, are listed with estimated value of the correlation function R (as defined in text). Real and imaginary parts of the transfer functions are listed with estimated errors in these quantities.

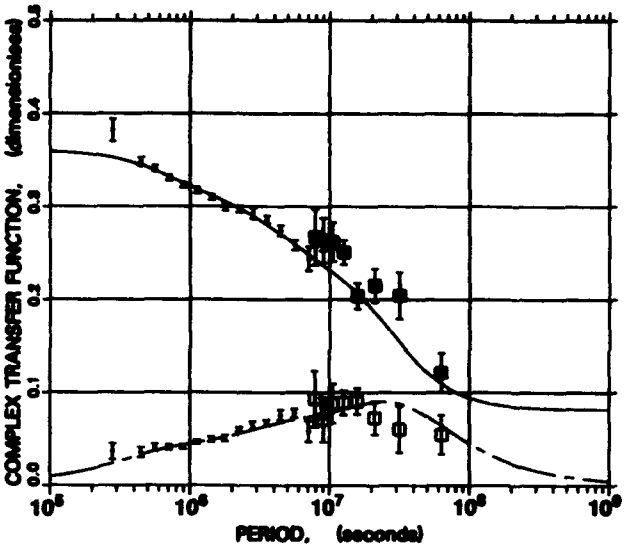

Figure 12. Complex transfer function (T) plotted against period. Solid squares are the real part of T, and open squares are the imaginary part of T as determined in this study and tabulated in Table 6. Solid circles are the real part of T, and open circles are the imaginary part of T as computed from data given by *Constable* [1993]. The solid and dashed curves are the real and imaginary part of T, respectively, computed from equation (8).

D, E, and F are sufficient to ensure that the transfer function satisfies causality. The best fit was found for time constants $A = 0.4399$ year, $B = 0.02926$ year, $C = 0.004079$ year, $D = 0.1479$ year, $E = 0.02287$ year, $F = 0.003529$ year. The real and imaginary parts of this transfer function are plotted in Figure 12 as solid and dashed curves, respectively.

The transfer function $T(s)$ given by (8) can be expanded as

$$T(s) = 0.0818 + \alpha sD/(1 + sD) + \beta sE/(1 + sE) + \gamma sF/(1 + sF), \quad (9)$$

where the time constants D, E, and F have the same values as for (8) and the constants α, β, and γ are $\alpha = 0.1527$, $\beta = 0.0741$, and $\gamma = 0.0513$.

The response of $T(s)$ to a unit step function in the external field $E(t)$ at $t = 0$ is the internal field $I(t)$ given by

$$I(t) = 0.0818 + 0.1527 \exp(-t/D) + 0.0741 \exp(-t/E) + 0.0513 \exp(-t/F) \quad (10)$$

where t is time and D, E, and F have the same values as for (8). $E(t)$ is the magnitude of the uniform external field and $I(t)$ is the magnitude of the induced dipole field at the geomagnetic equator. Equation (10) is valid for $t > 0$; $I(t) = 0$ for $t < 0$. In units of days, the time constants are $D = 54.0$ days, $E = 8.4$ days, and $F = 1.29$ days.

Equation (10) is applicable for a superconducting core and a mantle that is an insulator above a depth of 660 km. Since the core is not a superconductor, the constant term 0.0818 in (10) should be expected to decay with a time constant of a few thousand years. Since the mantle above 660 km is not an insulator, an additional term should be included in (10). The

additional term is approximately 0.1401 exp $(-t/G)$, where G is of the order of 1 hour. The coefficient 0.1401 in the additional term ensures that $I(0^+) = 0.5$, in agreement with (4), where 0^+ indicates a limit as t approaches 0 from the right.

Conclusions

First differences of magnetic observatory monthly means for years 1963–1982 have been analyzed using techniques of spherical harmonic analysis and power spectral analysis. Except for Earth's auroral regions, the external source signal is primarily zonal in geomagnetic coordinates. The spectrum of the external source signal consists of lines at 1 and 2 c/yr superimposed on a continuous spectrum. The continuous spectrum is well represented by zonal degree 1 spherical harmonics. The annual spectral line is primarily zonal degree 2; however, the annual line also includes small but significant spherical harmonics of other degrees and orders. The semiannual line is primarily zonal degree 1 but includes a significant zonal degree 3 harmonic, as well as smaller harmonics of other degrees and orders. The non-degree 1 harmonics and part of the degree 1 harmonic for the annual and semiannual line spectra are due to ionospheric current systems. The continuous spectrum for the frequency range studied is due primarily to the ring current and magnetopause currents, except for the auroral regions where ionospheric currents dominate.

The continuous spectrum, with annual and semiannual spectral lines excluded, has been used in this paper to estimate a global geomagnetic response function for periods ranging from 2 months to 2 years and sensitive to average radial electrical conductivity of the deep mantle down to the core-mantle boundary. The estimated response function found here agrees well with the values given by *Constable* [1993] for the narrow range of frequencies where the estimates overlap. The response function found here also agrees well with the value found by *McLeod* [1992] for a 2-year period and with the response for the conductivity profile proposed by *Banks* [1969] as described by *Achache et al.* [1981] for which conductivity at the core-mantle boundary is about 10 S/m.

Because the continuous spectrum is primarily zonal degree 1, this spectrum is well suited for estimation of a global geomagnetic response function. Neither the annual nor semiannual spectral lines are due to a single spherical harmonic. The annual line is mainly due to ionospheric currents, while the semiannual line contains a significant contribution from ionospheric currents. Since neither line can be modeled as well as the continuous spectrum using available magnetic observatory monthly means, these lines are not well suited for estimation of a global geomagnetic response function. Attempts by some previous investigators to use these lines, particularly the semiannual line, have resulted in large errors in estimates of the global response function at these frequencies, as is apparent in graphs of measured global response function shown by *Achache et al.* [1981]. A further advantage to using the continuous spectrum for estimating a global response function is that this method permits estimation of correlation between internal and external source signals; thus errors in the estimated response function can readily be estimated.

Estimation of the global response function at frequencies less than 2 c/yr is subject to larger relative errors than estimation of the response at higher frequencies, for several reasons. First, the power spectral density of the external source signal is less below 2 c/yr than above this frequency. Second, the induced internal source signal is smaller relative to the inducing signal at the lower frequencies. Third, possible error sources, such as core source signals that are not due to induction and ionospheric source signals that are not modeled by the spherical harmonic analysis, can reasonably be expected to be larger at low frequencies; in particular, ionospheric signals at the sunspot frequency and its harmonics can be expected. Nevertheless, improvements to the estimate for the global response function may be possible by using more recent observatory data than is available from the National Geophysics Data Center on the compact disk NGDC01. Also, it may be possible to obtain observatory data not presently available from the National Geophysics Data Center. Using a longer time interval could possibly result in some improvement, although the data quality is not as good for years prior to the time interval used for this study.

Although the response function found here agrees well with the response for the conductivity profile proposed by *Banks* [1969], as discussed by *Achache et al.* [1981], the question of uniqueness of the conductivity profile compatible with the estimated response function has not been explored in depth and is beyond the scope of this article. Some scientists have proposed a very thin, highly conducting layer in the mantle adjacent to the core-mantle boundary. Such a layer is compatible with the estimated response, since such a layer would have the same small effect on the global response as a small increase in the core radius. Investigation of the existence of such a thin layer appears to require use of signals originating within the core, such as geomagnetic jerks. The sharpness of the jerks observed at many observatories appears to be compatible with the time constants found here for the global response function; nevertheless, further research on this subject is desirable.

Note added in proof. The transfer function $W(s)$ corresponding to $T(s)$ given by equation (8) is, using equation (6),

$$W(s) = 0.773[(1 + sa)(1 + sb)(1 + sc)] \div [(1 + sd)(1 + se)(1 + sf)] \quad (11)$$

with time constants $a = 0.09691$ year, $b = 0.01637$ year, $c = 0.002521$ year, $d = 0.1690$ year, $e = 0.02422$ year, $f = 0.003665$ year. The admittance function $c(s)$ is $W(s)$ multiplied by 3186 km. *Weidelt* [1972] and *Parker* [1980] have discussed admittance functions of this type with interlaced real poles and zeros. For a flat Earth approximation, the vertical conductivity profile is a finite comb of positive delta functions. *Parker* [1980] has shown that the depths and magnitudes of these delta functions can be found from a continued fraction expansion of the admittance function. The depths and conductivity integrals for the delta function vertical conductivity profile corresponding to equation (11) for the flat Earth approximation is shown in Table 7a. The radial conductivity profile for a spherical Earth model also consists of delta functions. This radial conduc-

Table 7a. Delta Function Radial Conductivity Model Corresponding to the Transfer Function Shown in Figure 12: Flat Earth Approximation

	Depth, km	Conductivity Integral, S
1	656.1	0.258×10^6
2	1112.1	1.076×10^6
3	1731.7	4.139×10^6
4	2462.6	infinite

Table 7b. Delta Function Radial Conductivity Model Corresponding to the Transfer Function Shown in Figure 12: Spherical Earth Model

	Depth, km	Conductivity Integral, S
1	661.0	0.252×10^6
2	1138.0	1.001×10^6
3	1843.6	3.381×10^6
4	2886.0	infinite

Table 7c. Spherical Shell Radial Conductivity Model Corresponding to the Transfer Function Shown in Figure 12

	Depth, km	Conductivity, S/m
1	0–660	0
2	660–900	1.06
3	900–1490	1.69
4	1490–2886	2.42
5	2886–6371	infinite

tivity profile can be found from the vertical conductivity profile for the flat Earth approximation using equations given by *Weidelt* [1972]. This radial conductivity profile is shown in Table 7b.

A delta function radial conductivity model is not physically very realistic; the distance between delta functions in the model simply reflects achievable radial spatial resolution. A spherical shell model with nearly the same transfer function is shown in Table 7c. The shell boundaries were chosen midway between the delta functions of Table 7b, except the outer boundaries for the three center shells are at the 660-km phase transition and at the 2886-km core-mantle boundary. The conductivities shown in Table 7c were found by requiring the conductivity integral for each shell to equal the corresponding conductivity integrals of Table 7b. If one associates the conductivities of Table 7c with the shell midpoints, then by linear extrapolation one finds conductivities of 0.88 S/m at the 660-km phase transition and 2.94 S/m at the core-mantle boundary. The conductivities found here are reasonably consistent with those found by *Constable* [1993] and with conductivities found in laboratory studies discussed by *Constable* [1993].

Acknowledgment. This research was sponsored by the Office of Naval Research through program element 0601153N; H. C. Eppert, Jr., was the program manager. Contribution NRL/JA/7442/93/0012.

References

Achache, J., J. L. Le Mouël, and V. Courtillot, Long-period geomagnetic variations and mantle conductivity: An inversion using Bailey's method, *Geophys. J. R. Astron. Soc.*, *65*, 579–601, 1981.

Backus, G. E., Application of mantle filter theory to the magnetic jerk of 1969, *Geophys. J. R. Astron. Soc.*, *74*, 713–746, 1983.

Banks, R. J., Geomagnetic variations and the electrical conductivity of the upper mantle, *Geophys. J. R. Astron. Soc.*, *17*, 457–487, 1969.

Campbell, W. H., R. Schiffmacher, and H. W. Kroehl, Global quiet day field variation model WDCA/SQ1, *Eos Trans. AGU*, *70*, 66–74, 1989.

Constable, S., Constraints on mantle electrical conductivity from field and laboratory measurements, *J. Geomagn. Geoelectr.*, *45*, 707–728, 1993.

Currie, R. G., The geomagnetic spectrum—40 days to 5.5 years, *J. Geophys. Res.*, *71*, 4579–4598, 1966.

Ducruix, J., V. Courtillot, and J. L. Le Mouël, The late 1960's secular variation impulse, the eleven year magnetic variation and the electrical conductivity of the deep mantle, *Geophys. J. R. Astron. Soc.*, *61*, 73–79, 1980.

Eckhardt, D., K. Larner, and T. Madden, Long-period magnetic fluctuations and mantle electrical conductivity estimates, *J. Geophys. Res.*, *68*, 6279–6286, 1963.

Gardner, W. A., *Statistical Spectral Analysis*, Prentice-Hall, Englewood Cliffs, N. J., 1988.

Lowes, F. J., Mean square values on sphere of spherical harmonic vector fields, *J. Geophys. Res.*, *71*, 2179, 1966.

Marple, S. L., Jr., *Digital Spectral Analysis with Applications*, Prentice-Hall, Englewood Cliffs, N. J., 1987.

Matsushita, S., Solar quiet and lunar daily variation fields, in *Physics of Geomagnetic Phenomena*, vol. 1, edited by S. Matsushita and W. H. Campbell, pp. 301–424, Academic, San Diego, Calif., 1967.

McDonald, K. L., Penetration of the geomagnetic secular field through a mantle with variable conductivity, *J. Geophys. Res.*, *62*, 117–141, 1957.

McLeod, M. G., Geomagnetic Jerks and Temporal Variation, in *Encyclopedia of Earth System Science*, vol. 2, edited by W. A. Nierenberg, pp. 263–276, Academic, San Diego, Calif., 1991.

McLeod, M. G., Signals and noise in magnetic observatory annual means: Mantle conductivity and jerks, *J. Geophys. Res.*, *97*, 17,261–17,290, 1992.

Otnes, R. K., and L. Enochson, *Applied Time Series Analysis*, John Wiley, New York, 1978.

Parker, R. L., The inverse problem of electromagnetic induction: Existence and construction of solutions based on incomplete data, *J. Geophys. Res.*, *85*, 4421–4428, 1980.

Potemra, T. A., Magnetospheric currents, in *Encyclopedia of Earth System Science, vol. 3, edited by W. A. Nierenberg, pp. 75–84, Academic, San Diego, Calif., 1991.*

Roberts, R. G., The long-period electromagnetic response of the earth, *Geophys. J. R. Astron. Soc.*, *78*, 547–572, 1984.

Russell, C. T., On the occurrence of magnetopause crossings at 6.6 R_e, *Geophys. Res. Lett.*, *3*, 593–596, 1976.

Russell, C. T., and J. G. Luhmann, Solar-terrestrial interaction, in *Encyclopedia of Earth System Science*, vol. 4, edited by W. A. Nierenberg, pp. 279–288, Academic, San Diego, Calif., 1991.

Schultz, A., and J. C. Larsen, On the electrical conductivity of the mid-mantle, 1, Calculation of equivalent scalar magnetotelluric response functions, *Geophys. J. R. Astron. Soc.*, *88*, 733–761, 1987.

Schuster, A., The diurnal variation of terrestrial magnetism, with an appendix by H. Lamb, On the currents induced in a spherical conductor by variation of an external magnetic potential, *Philos. Trans. R. Soc. London, Ser. A*, *180*, 467–518, 1889.

Weidelt, P., The inverse problem of geomagnetic induction, *Z. Geophys.*, *38*, 257–289, 1972.

M. G. McLeod, Naval Research Laboratory, MC 7442, Stennis Space Center, MS 39529-5004. (e-mail: mcleod@mdff.span.nasa.gov)

(Received June 21, 1993; revised January 18, 1994; accepted March 17, 1994.)